Brain Structure and Function (2025) 230:114
https://doi.org/10.1007/s00429-025-02975-9

ORIGINAL ARTICLE

"Touching" the brain: braille reading mitigates the SC–FC decoupling of brain networks in congenital blindness

Saiyi Jiao[1,2] · Ke Wang[1] · Jiahong Zeng[1] · Zhenjiang Cui[1] · Yudan Luo[1,3] · Zaizhu Han[1]

Received: 4 April 2025 / Accepted: 18 June 2025 / Published online: 7 July 2025

Abstract

Acquired experiences are crucial for brain structure and function development, with a strong covariance between them. However, how experience deprivation reorganizes the covariance between structural connectivity (SC) and functional connectivity (FC), and how newly acquired experience influences this plastic reorganization remain unclear. To address these, we recruited 21 congenitally blind (CB) participants and 21 normally sighted (NS) controls. Using multi-modal MRI and graph-theoretical analyses, we examined the topological properties, and then investigated the SC–FC coupling reorganization and its relationship with braille reading ability. Compared to the NS group, the CB group showed significant topological reorganization in structural networks and disrupted intra-hemispheric SC–FC coupling. Importantly, braille reading proficiency and earlier braille onset mitigated SC–FC decoupling, suggesting that braille reading partially rescued disrupted network. Our findings highlight dynamic network plasticity in compensating for visual loss, and underscore the importance of early braille acquisition in maintaining brain networks stability in congenital blindness.

Keywords SC–FC coupling · Braille reading · Plastic network reorganization · Multi-modal MRI · Congenital blindness

Introduction

Acquired experiences continuously shape the structure and function of the human brain, enabling it to adapt to environmental constraints or changes (McKenzie et al. 2014; Sampaio-Baptista and Johansen-Berg 2017; Greenough et al. 1987; Kolb and Age 1998). Humans primarily perceive the world through the visual pathway (Ungewiss et al. 2020; Joukal 2017), and as such, visual experience significantly influences brain plasticity (Greenough et al. 1987; Kolb and Age 1998; Li et al. 2022). Furthermore, the structural connectivity (SC) and functional connectivity (FC) in the human brain do not develop independently; instead, they exhibit robust covariation within the individual brain (Mišić et al. 2016). Thus, investigating the impacts of visual experience deprivation and newly acquired cognitive abilities (e.g., braille reading ability through touching braille dot patterns to acquire tactile linguistic experience) on the covariation of SC and FC can greatly help us to "touch" the brain plasticity.

Neuronal populations form brain regions and their interconnecting white matter structures (Hagmann et al. 2008; Sarwar et al. 2021). Within the constraints of white matter SC, extensive neural co-activation patterns between brain regions are referred to as FC (Damoiseaux et al. 2006). SC serves as the physiological mechanism for information transfer between brain regions, maintaining and constraining FC at multiple scales (Palop and Mucke 2016; Park and Friston 2013; Suárez et al. 2020), while FC continuously influences and reshapes SC through brain plasticity (Honey et al. 2009). Recent advances in non-invasive multi-modal magnetic resonance imaging (MRI) techniques [e.g., diffusion tensor imaging (DTI) and resting-state functional MRI (rs-fMRI)] along with brain network analysis methods (Honey et al. 2010), have made it possible to quantitatively measure SC and FC (Damoiseaux and Greicius 2009) and explore their covariation (i.e., SC–FC coupling). Compared

✉ Zaizhu Han
zzhhan@bnu.edu.cn

1 National Key Laboratory of Cognitive Neuroscience and Learning & IDG/McGovern Institute for Brain Research, Beijing Normal University, Beijing 100875, China

2 Department of Otorhinolaryngology, Peking Union Medical College Hospital, Beijing 100730, China

3 Department of Psychology and Art Education, Chengdu Academy of Educational Sciences, Chengdu 610036, China

to single-modal MRI analysis, SC–FC coupling analysis based on multi-modal MRI can capture subtle changes in the brain, aiding in investigating the constraining and maintaining mechanisms of structural networks on functional networks (Avena-Koenigsberger et al. 2017), as well as revealing the plastic modulation of functional networks on structural network. Research on SC–FC coupling contributes to a more precise understanding of the relationship between dynamic structural changes and the integration of information in brain networks.

Extensive research has demonstrated a close SC–FC coupling in healthy individuals (Honey et al. 2010; Vázquez-Rodríguez et al. 2019; Pinotsis et al. 2013; Gu et al. 2021), with the strength of SC–FC coupling being associated with the acquisition of cognitive abilities, such as executive function and working memory (Suárez et al. 2020; Vázquez-Rodríguez et al. 2019). SC–FC coupling has also been widely studied in special populations with diseases (Wu et al. 2023; Pan et al. 2023; Chen et al. 2021a, c; Zhang et al. 2019a, b). Diseases not only cause changes in brain structure and function, but also alter the degree of SC–FC coupling, which is related to clinical indicators (Wu et al. 2023; Hagmann et al. 2010; Huang and Ding 2016; Cao et al. 2020; Chiang et al. 2015; Heuvel et al. 2013; Wang et al. 2021) and changes in cognitive abilities (Medaglia et al. 2018; Kuceyeski et al. 2016). SC–FC coupling can distinguish diseased populations from healthy individuals, and identify recovery mechanisms in brain networks after diseases onset (Romero-Garcia et al. 2014), which is crucial for prognosis.

Investigating brain reorganization in the blind population offers valuable insights into the nature of brain plasticity. However, previous studies have often focused on changes within structural networks (Li et al. 2013; Shu et al. 2009a, b; Zhou et al. 2022) or resting-state functional networks (Hou et al. 2017; Pelland et al. 2017), often using single-modality imaging. There is lacking of research on how visual experience deprivation influences SC–FC coupling. Existing SC–FC studies in other populations include topological analysis of structural and functional networks as a prerequisite for SC–FC coupling investigations (Zhang et al. 2019a, b; Chen et al. 2021a, c, 2022). This quality-control step confirms that the reconstructed networks satisfy essential neurobiological criteria (e.g., small-worldness topology), thus validating the foundation for core coupling analyses. Considerable evidence exists concerning topological properties of brain networks in blind populations. Specifically, in terms of structural networks in blind individuals, studies have shown a decrease in network efficiencies (Li et al. 2013; Shu et al. 2009a, b; Zhou et al. 2022), along with an increase in characteristic path length (Shu et al. 2009a, b; Zhou et al. 2022). In the resting-state functional networks, no evidence has been observed regarding the reorganization of topological properties of the blind population. Moreover, most previous studies on brain networks in blind individuals recruited early blind participants, making it difficult to exclude the influence of early visual experience on brain structure and function.

Braille reading ability, as a newly acquired cognitive ability in blind individuals, plays an important role in the plastic brain reorganization of blind individuals (Sadato et al. 1996; Hamilton et al. 2000; Burton et al. 2002, 2012). Additionally, there is a strong association between cognitive ability and SC–FC coupling. A stronger SC–FC coupling typically supports an enhanced cognitive processing (Suárez et al. 2020; Vázquez-Rodríguez et al. 2019; Popp et al. 2024; Wang et al. 2015a, b). And decoupled SC–FC observed in disorders (Pan et al. 2023; Zhang et al. 2019a, b; Chen et al. 2021a, c; Wang et al. 2015a, b) was related with the cognitive impairment (Pan et al. 2023; Medaglia et al. 2018; Kuceyeski et al. 2016). Therefore, newly acquired experience from braille reading in blind populations maybe a potential mechanism to maintain SC–FC relationships in reorganized networks, due to the experience-dependent plasticity. Addressing the relationship between braille reading and SC–FC coupling in blind populations offers considerable scientific attribution.

However, it remains unclear how the overall topological properties of structural and resting-state functional networks reorganize, and how SC–FC coupling changes due to the congenital visual experience deprivation. Additionally, braille reading is a unique and newly acquired cognitive ability for blind individuals, comparing with the normal sighted individuals. Previous evidence has demonstrated that the acquisition of braille reading influences the SC or FC of blind individuals (Jiao et al. 2023; Lin et al. 2022). Therefore, elucidating the relationship between reorganized SC–FC coupling and braille reading experience is of significant interest, but it remains poorly understood.

To address these issues, we recruited 21 congenitally blind (CB) participants and 21 perfectly matched normal sighted (NS) controls. High-resolution multi-modal MRI images were collected from all participants, along with behavioral data of a off-line braille reading task in the congenitally blind participants. First, we constructed the white matter structural network and resting-state functional network for each participant. Then, graph theoretical analysis was employed to examine topological alterations between the two groups, including small-world properties (i.e., clustering coefficient, C_p; characteristic path length, L_p; normalized C_p, γ, gamma; normalized L_p, λ, lambda; small-worldness, σ, sigma) and network efficiency properties (i.e., global efficiency, E_g; local efficiency, E_{loc}), for both structural and functional networks. Analyzing the topological

properties of structural and functional networks is essential for quality control of constructed networks, and provides a deeper understanding of plastic reorganization for each network. Finally, the SC–FC coupling analysis for networks in different levels, and its relationship with blindness-relevant measures were conducted (Fig. 1).

Methods

Participants

Twenty-one CB (7 females/14 males; age/years of blindness duration: $M=24.38$, $SD=5.32$ years) and 21 NS (11 females/10 males; age: $M=22.81$, $SD=2.58$ years) participants were recruited in the study. The two groups were carefully matched for age [$t_{(40)}=1.22$, $P=0.23$] and sex [$\chi^2_{(1)}=0.89$, $P=0.35$]. The CB participants had been blind from birth, and were proficient in braille (years of braille experience: $M=17.24$, $SD=5.19$; age of braille onset: $M=8.14$, $SD=2.24$ years). They reported no experience with colors, shapes, or motion, with 13 having at most minimal light perception. All participants were right-handed (Oldfield 1971), had no known neurological or psychiatric disorders, and provided informed consent. Most of these participants have been reported in our recent studies (Jiao et al. 2023, 2024; Lin et al. 2022).

This study was approved by the Institutional Review Board of the National Key Laboratory of Cognitive Neuroscience and Learning, Beijing Normal University.

MRI data acquisition and preprocessing

For each participant, high-resolution T1-weighted images, DTI images, rs-fMRI images, and field map were acquired using a 3T Siemens Prisma scanner at the Imaging Center for Brain Research, Peking University. The field map was collected before the rs-fMRI scan, preparing for preprocessing of rs-fMRI images. The scanning parameters for each type of MRI were as follows. (1) T1-weighted images: magnetization-prepared rapid gradient-echo (MP-RAGE) sequence; 192 sagittal slices; echo time (TE)=2.98 ms; repetition time (TR)=2530 ms; inversion time (TI)=1100 ms; slice thickness=1 mm; voxel size=0.5×0.5×1.0 mm^3; flip angle=7°; and field of view (FOV)=256×256 mm^2. (2) DTI images: single-shot echo-planar imaging (EPI) sequence; 70 axial slices; TE=73 ms; TR=5100 ms; diffusion directions=30; b-value 1=0 s/

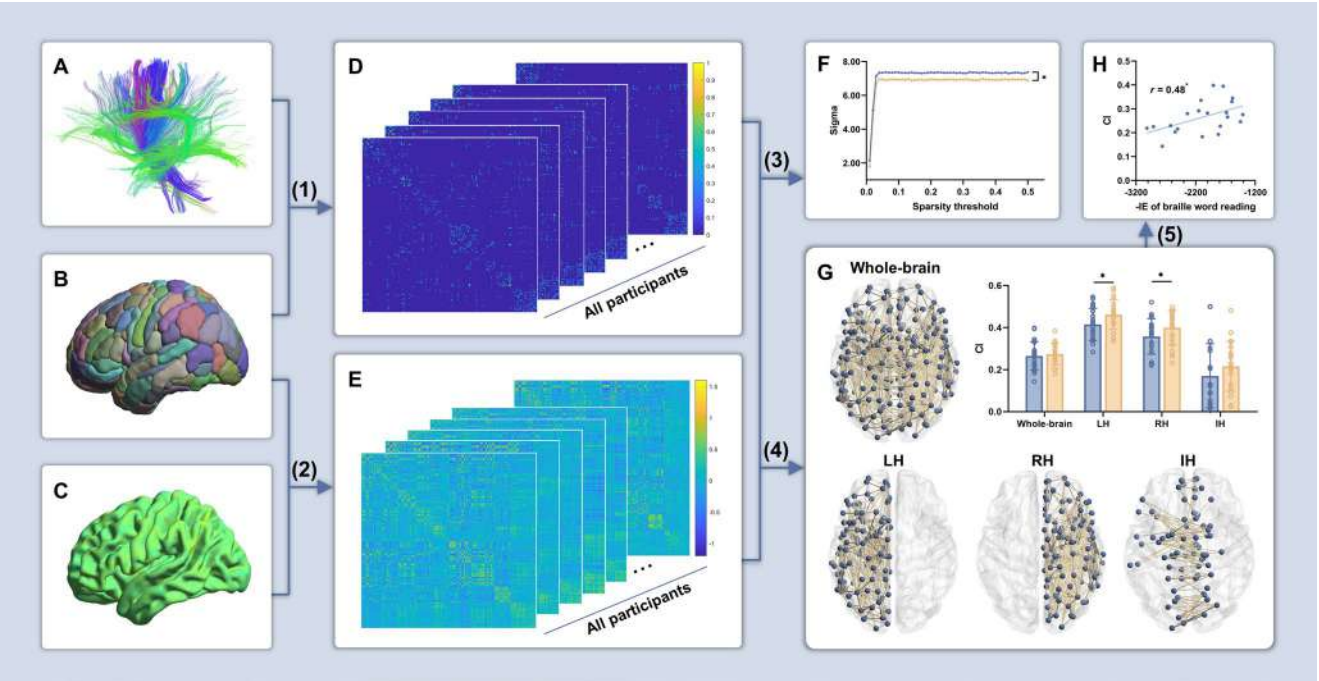

Fig. 1 Schematic flowchart for data analysis. (1) The construction of structural networks (D) were conducted by determining the white matter fibers (A) between each pair nodes in Brainnetome Atlas (B). (2) The resting-state functional networks (E) were constructed by obtaining the mean resting-state functional MRI time series (C) of each node in Brainnetome Atlas (B), and calculating the interregional functional connectivity. (3) Identification of topological properties exhibited significant group differences (F) both in structural networks (D) and structural networks (E). (4) Investigating the reorganization patterns in SC-FC coupling (G) for both whole-brain networks and hemispheric networks. (5) Clarifying the relationship between SC-FC coupling and blindness-relevant measures by performing the Spearman correlation analysis (H) across congenitally blind participants. *CI* coupling index; *FC* functional connectivity; *IH* inter-hemispheric networks; *LH* left hemispheric networks; *RH* right hemispheric networks; *SC* structural connectivity

mm^2; b-value 2 = 1000 s/mm^2; b-value 3 = 2000 s/mm^2; slice thickness = 2 mm; voxel size = 2.0 × 2.0 × 2.0 mm^3; flip angle = 60°; and FOV = 224 × 224 mm^2. (3) rs-fMRI images: lasting for 8.33 min; EPI sequence; 64 axial slices; TE = 30 ms; TR = 2000 ms; slice thickness = 2 mm; gap = 0.2 mm; voxel size = 2.0 × 2.0 × 2.0 mm^3; flip angle = 90°; and FOV = 224 × 224 mm^2. (4) field map: lasting for 2.42 min; 64 axial slices; TE1 = 4.92 ms; TR = 635 ms; slice thickness = 2 mm; voxel size = 2.0 × 2.0 × 2.0 mm^3, flip angle = 60°; and FOV = 224 × 224 mm^2. During the rs-fMRI scan and field map sequence, the participants were asked to remain awake and keep their eyes closed.

The DTI preprocessing was conducted using PANDA (Cui et al. 2013) (http://www.nitrc.org/projects/panda/), including the followign steps. (1) Brain extraction. (2) Correction for head motion, eddy current distortions, and *b*-matrix (Leemans and Jones 2009). (3) Computation of diffusion tensor metrics [i.e., fractional anisotropy (FA), axial diffusivity, mean diffusivity and radial diffusivity]. (4) Normalization to Montreal Neurological Institute (MNI) space and smoothing with a 6 mm Gaussian kernel.

The rs-fMRI preprocessing was performed using the Data Processing Assistant for Resting-State fMRI version 5.4 (DPARSF 5.4, http://rfmri.org/DPARSF), involving the following main steps. (1) Removal of the first 10 volumes of the time series. (2) Fieldmap correction to reduce the effects of field inhomogeneity. (3) Time-slicing correction and head motion realignment. Participants with head motion exceeding 2 mm translation and 2° rotation were excluded from the further analysis. (4) Coregistration of functional images with T1 images using the Diffeomorphic Anatomical Registration Through Exponentiated Lie Algebra (DARTEL) algorithm (Ashburner 2007). (5) Normalization to MNI space with a resampled voxel size of 1.5 × 1.5 × 1.5 mm^3 (1987). (6) Regression of nuisance covariates, including white matter signals, cerebrospinal fluid signals and Firston-24 head motion parameters. (7) Spatial smoothing with a 4 mm Gaussian kernel.

Network construction

To evaluate SC and FC, we constructed a white matter structural network and a resting-state functional network for each participant. The nodes of both networks were defined based on the 246 regions from the Brainnetome Atlas (Fan et al. 2016), with the edge definition procedures were described below (Fig. 1).

For the white matter structural networks, deterministic fiber tractography (Heuvel and Sporns 2011; Wang et al. 2018; Zhong et al. 2015) with fiber assignment by continuous tracking (FACT) algorithm (Mori et al. 1999; Mori and Zijl 2002) was used to reconstruct white matter fibers in the whole brain. Fiber tractography was terminated when the turning angle between two consecutive orientations exceeded 45° or FA was less than 0.20. The mean FA value of the interregional white matter tract was defined as the weighted edge of the structural network. For the resting-state functional networks, the mean rs-fMRI time series of each node were extracted, and the interregional correlation coefficients were calculated as the edge weights of the functional network.

As a result, two separate 246 × 246 symmetric weighted matrices were obtained for each participant, representing the SC and FC within the brain.

Topological properties of networks

Before investigating the SC–FC coupling, it is essential to first analyze the topological properties of each network (i.e., structural network and functional network) for the quality control of the constructed brain networks, providing a deeper understanding of plastic reorganization for each network, as well as to better understand the differences between congenital blind individuals and sighted controls. These analysis verified that the constructed brain networks in our study met fundamental neurobiological criteria, and ensured the reliability of the core issues to be addressed in subsequent analysis (i.e., SC–FC coupling). This analysis aids to reveal potential unique patterns of SC and FC in the CB group, shedding light on possible neural adaptations or reorganization mechanisms. Understanding these topological reorganizations provides a solid foundation for subsequent coupling analysis, allowing for a more precise exploration of the relationship between structural and functional networks and their variations across different groups.

To reveal the topological properties of whole-brain structural and functional networks, we calculated the small-world properties and network efficiency properties (Latora and Marchiori 2001) using the GRETNA toolbox (Wang et al. 2015a, b). A range of connection sparsity thresholds, from 0.01 to 0.5, with an interval of 0.01, was applied to both whole-brain structural and functional networks. The threshold range was established based on prior related researches (Chen et al. 2021a, b, 2022).

Small-world properties

Small-world properties included the C_p, L_p, γ, λ, σ. Small-world networks exhibit both high clustering coefficients and short characteristic path lengths, indicating that brain networks achieve a balance between local information processing and global information integration. The small-world network serves as a key model for characterizing complex brain networks, typically defined by the conditions: γ > 1 and

$\lambda \approx 1$ (Watts and Strogatz 1998), or $\sigma = \gamma/\lambda > 1$ (Humphries et al. 2006).

C_p reflects the local connectivity density of nodes within a network, indicating the extent to which a node's neighbors are interconnected. A high clustering coefficient reflects the tight connectivity among local neuronal groups, facilitating specialized information processing. It is calculated as the mean clustering coefficient of all nodes in the network:

$$C_p^G = \frac{1}{N}\sum_{i\in G} C_i = \frac{1}{N}\sum_{i\in G}\frac{2e_i}{k_i(k_i-1)}$$

where C_i is the local clustering coefficient of node i, e_i is the number of existing edges between node i and its neighbor nodes, k_i is the degree of node i, and N is the number of nodes in graph G.

L_p represents the average shortest path length between all pairs of nodes in a network, reflecting the efficiency of global information transfer. A shorter L_p ensures efficient communication between different brain regions, supporting complex cognitive functions. It is defined as follows:

$$L_p^G = \frac{1}{N}\sum_{i\in G} l_i = \frac{1}{N(N-1)}\sum_{i\in G}\sum_{i\neq j\in G} l_{ij}$$

where $l_i$is the average shortest path length from node i to all other nodes in the network, $l_{ij}$is the shortest path length from node j to node i, and N is the number of nodes in graph G.

γ is a measure of how clustered a network is relative to the random networks with the same size and degree distribution, which is calculated as:

$$\gamma^G = \frac{C_p^G}{C_p^{rand}}$$

where C_p^G is the clustering coefficient of the real graph G, and the C_p^{rand} is the mean clustering coefficient of the 100 random graphs (Maslov and Sneppen 2002; Milo et al. 2002).

λ measures the efficiency of global information transfer in the real network compared to the random networks with same size and degree distribution, which is calculated as:

$$\lambda^G = \frac{L_p^G}{L_p^{rand}}$$

where L_p^G is the clustering coefficient of the real graph G, and the L_p^{rand} is the mean clustering coefficient of the 100 random graphs.

σ quantifies the small-worldness of the brain network by comparing the to the γ to the λ. For small-world networks, $\sigma > 1$ indicating high clustering and short path lengths. The σ of graph G is calculated as follows:

$$\sigma^G = \frac{\gamma^G}{\lambda^G}$$

Network efficiency properties

The network efficiencies of brain networks were evaluated by the E_g and E_{loc}. E_g and E_{loc} are employed to evaluate network efficiency because they reflect distinct aspects of information processing. E_g captures the overall information transfer capability across the entire network, while E_{loc} focuses on the transfer efficiency within localized groups of nodes. Together, these measures offer a comprehensive view of both global and local network dynamics.

E_g is a global metric used to measure the overall communication efficiency of parallel information transfer in a network, and a higher value means that it is easier and faster to transfer information between the nodes in the network. E_g is calculated as the mean of the reciprocal of the shortest path between all pairs of nodes in the network:

$$E_g^G = \frac{1}{N(N-1)}\sum_{i\in G}\sum_{j\neq i\in G}\frac{1}{L_{ij}}$$

where L_{ij} is the shortest path length between nodes i and j, and N is the number of nodes in graph G.

E_{loc} represents the communication efficiency of information transfer within the local environment, which reflects the average ability of a network to tolerate faults by measuring the communication efficiency among the nearest neighbors of the node when it is removed. This metric is defined as follows:

$$E_{loc}^G = \frac{1}{N}\sum_{i\in G} E_g^{G_i}$$

where G_i is the neighborhood subnetwork of node i composed of the nearest neighbors and their connections, and N is the number of nodes in graph G.

SC–FC coupling analysis

We comprehensively investigated the reorganization patterns of SC–FC coupling across whole-brain networks and hemispheric networks [i.e., left hemispheric (LH) network, right hemispheric (RH) network and inter-hemispheric (IH) network].

For SC and FC matrices of each participants, we excluded FC edges lacking corresponding white matter structural connections from the SC–FC coupling analysis. To accommodate the non-Gaussianity of the structural network, we calculated the Spearman correlation (*r* values) between SC matric and the corresponding FC matric across the existing edges (Gu et al. 2021). To improve normality, Fisher's *r*-to-*z* transformation was applied to the *r* values, yielding *z* values. The SC–FC CI was defined as the absolute *z* value (Zhao et al. 2019).

To further investigate blindness-relevant SC–FC coupling reorganization, the calculations described above were applied to both the whole-brain networks and hemispheric networks (Fig. 1). Specifically, the hemispheric networks included the LH, RH and IH networks. These were constructed by including edges connected by nodes restricted to the corresponding hemispheres.

Behavioral data collection and preprocessing

The braille word reading task was used to assess the braille reading ability of the CB participants. Participants completed the task in a quiet room, either before or after the MRI scanning session.

The task consists of 40 single Chinese characters (i.e., 20 nouns and 20 verbs; e.g., "喊" meaning shout, /han3/ with the pinyin indicating the tone of the preceding syllable) and 48 two-character Chinese words (i.e., 16 concrete words, 16 abstract words, and 16 function words; e.g., "电视" meaning television, /dian4shi4/). The selected 88 items includes low- to medium-frequency words, ensuring a good match with typical word frequency distributions. The stimuli were tactilely presented on a braille display device (THDZ-40, http://www.qhqmx.com.cn/index.html). Participants were asked to read the word as quickly as possible. For each item, the accuracy and RT of the first complete response were recorded.

To minimize the impact of outlier responses, trials with RTs deviating by more than two standard deviations from the mean RT across all trials were excluded for each participant. The -IE measure was used to access behavioral performance, accounting for potential trade-off effects between speed and accuracy. The IE was computed as the ratio of the average RT for correct items to the overall accuracy across all items (Townsend et al. 1983). A higher -IE indicated better performance on the task.

Statistical analysis

To identify blindness-relevant changes in topological properties, we performed permutation correction (1000 times, $P<0.05$) by the MATLAB package EPEPT (Knijnenburg et al. 2009) for each topological metric between the two groups. This analysis was conducted not only for each sparsity level but also for the AUC across the full range of sparsity thresholds.

Additionally, to reveal blindness-relevant changes in SC–FC coupling, we compared the CI values between the two groups using a permutation correction (1000 iterations, $P<0.05$) for both whole-brain networks and each hemispheric network.

Finally, to explore the relationship between SC–FC coupling index (CI) and acquired braille reading ability in the CB participants, we performed a Spearman correlation analysis between the blindness-relevant measures (i.e., age of braille onset, -IE of reading task, years of blindness duration) and the CI values of the whole-brain networks and each hemispheric network across CB participants (Fig. 1; *FDR* corrected, $P<0.05$).

Notably, framewise displacement (FD) (Jenkinson et al. 2002) values did not differ significantly between groups [$t_{(40)}=0.38$, $P=0.70$], and subsequent correlation analyses confirmed no significant associations between FD and either SC–FC coupling or blindness-related measures ($Ps>0.07$), suggesting that in-scanner head motion did not confound our primary findings.

Results

Blindness-relevant changes of topological properties

The results are presented in Fig. 2; Table 1. Both the structural and functional networks exhibited small-world topology in both groups (Fig. 2A; $\gamma>1$, $\lambda\approx1$, $\sigma>1$). Significant group differences in topological properties were observed in the structural networks, both for each sparsity threshold (Fig. 2A, Supplementary Tables 1, 2; L_p: permutation-corrected $Ps<0.03$; γ: permutation-corrected $Ps<0.02$; σ: permutation-corrected $Ps<0.03$; E_g: permutation-corrected $Ps<0.05$) and for the area under the curve (AUC) across the sparsity range (Fig. 2B; Table 1; L_p: permutation-corrected $P=0.02$; γ: permutation-corrected $P=0.01$; σ: permutation-corrected $P=0.007$; E_g: permutation-corrected $P=0.03$). Specifically, compared to the NS group, the CB group showed a significant increase in three small-world properties (i.e., L_p, γ, σ) and a reduction in E_g. No significant group differences were found in other properties of the structural network or in any properties of the functional networks at all defined sparsity thresholds (Fig. 2A, Supplementary Tables 1, 2) and AUC (Fig. 2B; Table 1) (permutation-corrected $Ps>0.05$). Detailed topological properties data for

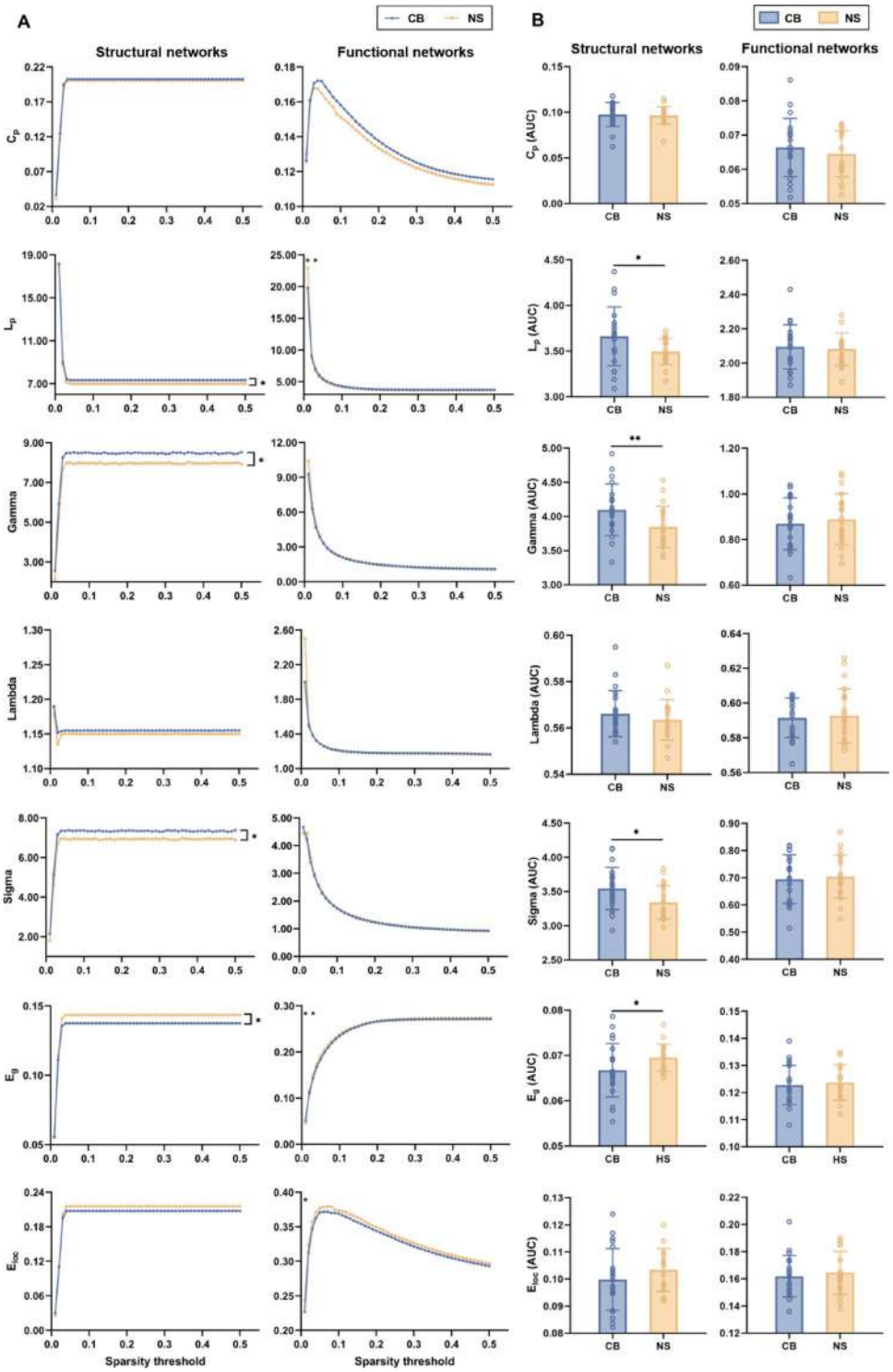

Fig. 2 Group comparisons of the topological properties for both structural networks and functional networks under all sparsity thresholds (**A**) and the AUC (**B**). The asterisk with square brackets indicate that significant group differences in the current topological property were observed across almost all sparsity thresholds. The circles in AUC represent the individual data. Error bars indicate the standard deviation. Permutation corrected: $^{**}P<0.01$; $^{*}P<0.05$. *AUC* area under the curve; *CB* congenitally blind group; C_p clustering coefficient; E_g global efficiency; E_{loc} local efficiency; L_p characteristic path length; *NS* normally sighted group

each defined sparsity threshold are shown in Supplementary Tables 1, 2.

Blindness-relevant changes of SC–FC coupling

The results are shown in Fig. 3; Table 2. Regarding the whole-brain networks, we did not observed any significant group differences in the SC–FC CI values (permutation-corrected $P=0.33$). However, for the hemispheric brain networks, significant reorganization of SC–FC coupling were found in the LH and RH networks, but not in the IH network (LH: permutation-corrected $P=0.02$; RH: permutation-corrected $P=0.05$; IH: permutation-corrected $P=0.13$).

Table 1 Topological properties of the whole-brain structural and functional networks for the area under the curve (AUC)

	Topological properties (AUC)						
	C_p	L_p	γ	λ	σ	E_g	E_{loc}
Structural networks							
CB	0.098 (0.013)	3.661 (0.313)	4.098 (0.366)	0.566 (0.010)	3.547 (0.300)	0.067 (0.006)	0.100 (0.011)
NS	0.097 (0.009)	3.496 (0.139)	3.846 (0.296)	0.564 (0.009)	3.344 (0.238)	0.070 (0.003)	0.103 (0.008)
P value	0.40	**0.03***	**0.009****	0.18	**0.01***	**0.03***	0.13
Functional networks							
CB	0.066 (0.008)	2.093 (0.126)	0.869 (0.110)	0.592 (0.011)	0.695 (0.087)	0.123 (0.007)	0.162 (0.015)
NS	0.065 (0.007)	2.082 (0.092)	0.889 (0.108)	0.593 (0.015)	0.704 (0.077)	0.124 (0.007)	0.165 (0.015)
P value	0.22	0.36	0.26	0.36	0.37	0.30	0.29

Permutation-corrected: **$P<0.01$; *$P<0.05$. Significant results (permutation-corrected $P < 0.05$) indicated in bold. *CB* congenitally blind group; C_p, clustering coefficient; E_g, global efficiency; E_{loc} local efficiency; L_p characteristic path length; *NS* normally sighted group; *γ* gamma, normalized clustering coefficient; *λ* lambda, normalized characteristic path length; *σ* sigma, small-worldness

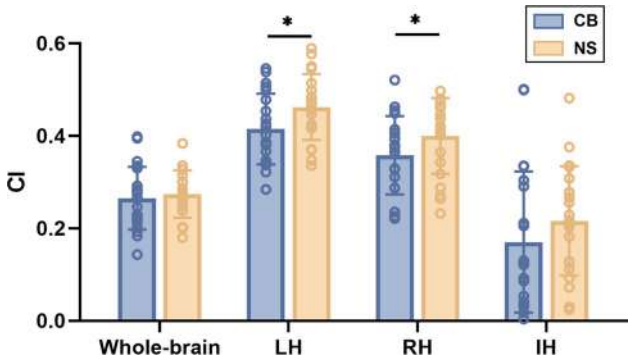

Fig. 3 Group comparisons of the SC–FC coupling index (CI) for both whole-brain networks and hemispheric networks. The circles represent the individual data. Error bars indicate the standard deviation. Permutation corrected: *$P<0.05$. *CB* congenitally blind group; *FC* functional connectivity; *IH* inter-hemispheric networks; *LH* left hemispheric networks; *NS* normally sighted group; *RH* right hemispheric networks; *SC* structural connectivity

Table 2 SC–FC coupling index values for both the whole-brain networks and hemispheric networks

	Whole-brain networks	Hemispheric networks		
		LH	RH	IH
CB	0.27(0.07)	0.41(0.07)	0.36(0.08)	0.17(0.15)
NS	0.27(0.05)	0.46(0.07)	0.40(0.08)	0.22(0.12)
P value	0.33	0.02*	0.05*	0.13

Permutation-corrected: *$P<0.05$. *CB* congenitally blind group; *FC* functional connectivity; *IH* inter-hemispheric networks; *LH* left hemispheric networks; *NS* normally sighted group; *RH* right hemispheric networks; *SC* structural connectivity

Specifically, the CI values of LH and RH networks were lower than in the CB group compared to the NS group.

Correlation between blindness-relevant measures and SC–FC coupling

In the braille word reading task, the CB individuals demonstrated high accuracy (M = 0.97, SD = 0.02). The mean reaction time (RT) was 2019.26 ms (SD = 473.07 ms) and the mean negated inverse efficiency (-IE) value was −2078.76 (SD = 488.25). Figure 4; Table 3 show the results of correlation analysis between blindness-relevant measures (i.e., age of braille onset, -IE of reading task, years of blindness duration) and the SC–FC CI values across CB participants. Specifically, the age of braille onset was negatively correlated with the SC–FC CI values in the whole-brain, LH, and RH networks [Figure 4A; whole-brain networks: $r = -0.63$, *false discovery rate (FDR)* corrected $P = 0.01$; LH networks: $r = -0.61$, *FDR* corrected $P = 0.01$; RH networks: $r = -0.49$, *FDR* corrected $P = 0.05$]. Performance of braille word reading task was positively correlated with SC–FC CI values of whole-brain and LH networks (Fig. 4B; whole-brain networks: $r = 0.48$, *FDR* corrected $P = 0.04$; LH networks: $r = 0.44$, *FDR* corrected $P = 0.05$). Additionally, SC–FC CI values in the LH networks were negatively correlated with the years of blindness duration (Fig. 4C; $r = -0.46$, *FDR* corrected $P = 0.05$).

These findings indicate that a longer duration of blindness is asssociated with greater SC–FC decoupling, while the acquisition of braille reading ability appears to mitigate this effect. Specifically, CB individuals, who learned braille at an earlier age or exhibited higher proficiency in braille reading, showed weaker SC–FC decoupling.

Discussion

By utilizing multi-modal MRI technologies and graph-theoretic analytical approaches, this study revealed the reorganized patterns of topological properties and SC–FC coupling in the structural networks and functional networks after congenitally visual deprivation. Additionally, we revealed that the acquisition of braille reading cognitive ability mitigated the degree of disrupted SC–FC coupling in congenital blindness. Our findings further elucidated the dynamic plasticity induced by congenitally visual loss on brain networks, thereby enhancing our understanding of brain plasticity at the network level.

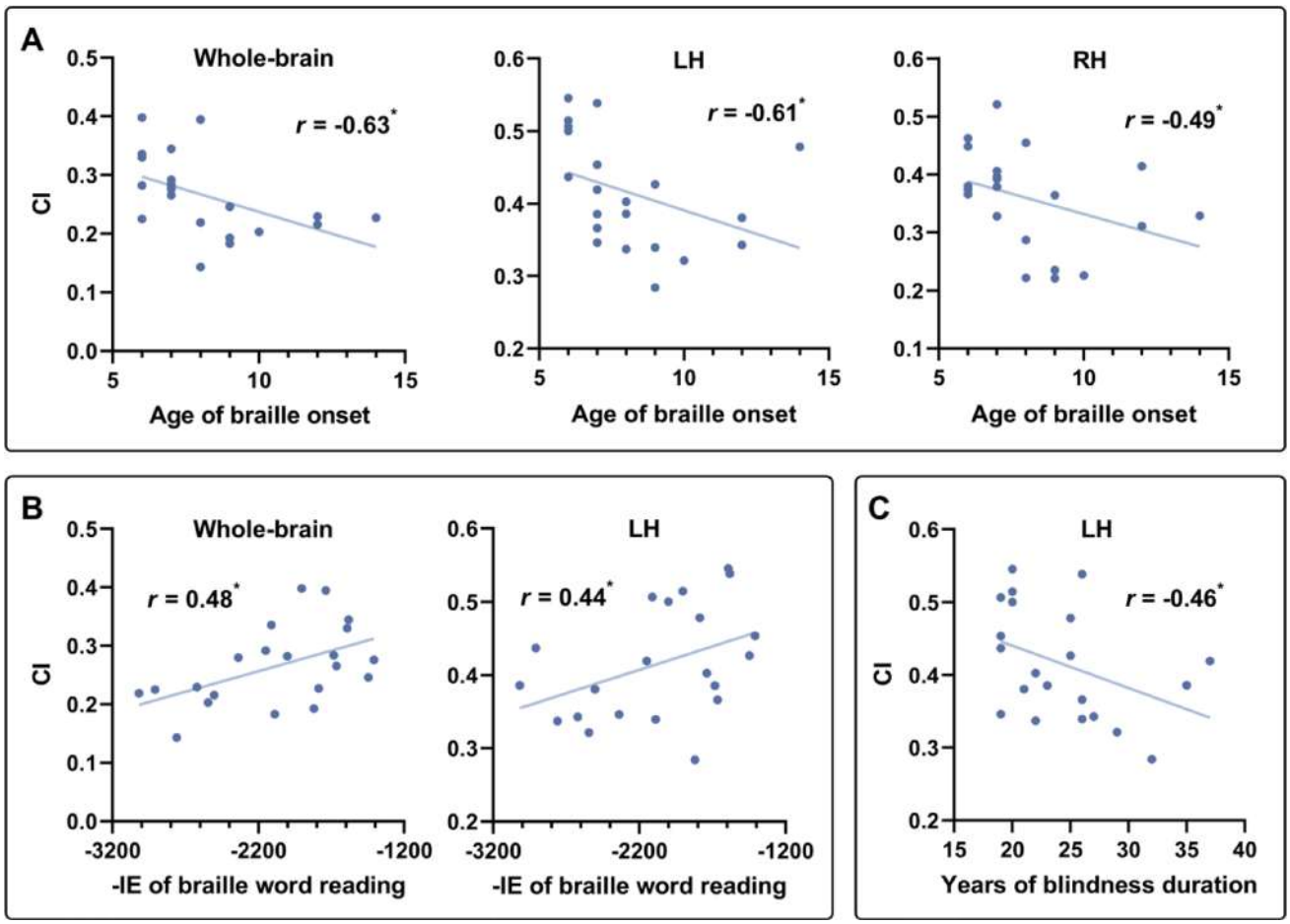

Fig. 4 Significant correlations between SC–FC coupling index (CI) and blindness-relevant measures [i.e., age of braille onset (**A**), performance of braille word reading task (**B**), and years of blindness duration (**C**)] in congenitally blind group. *FDR* Corrected: $*P<0.05$. *FC* functional connectivity; *IH* inter-hemispheric networks; *LH* left hemispheric networks; *RH* right hemispheric networks; *SC* structural connectivity

Table 3 The correlation coefficients of SC–FC coupling index (CI) and blindness-relevant measures (i.e., age of braille onset, performance of braille word reading task, and years of blindness duration)

	CI			
	Whole-brain	LH	RH	IH
Age of braille onset	− 0.63*	− 0.61*	− 0.49*	− 0.36
-IE of braille work reading	0.48*	0.44*	0.41	− 0.08
Years of blindness duration	− 0.34	− 0.46*	− 0.35	− 0.19

FDR Corrected: $*P<0.05$. *FC* functional connectivity; *IH* inter-hemispheric networks; *LHnull* left hemispheric networks; *RH* right hemispheric networks; *SC* structural connectivity

Plastic reorganization of topological properties after congenitally visual loss

The small-world property represents an optimal organizational structure for brain network, enabling efficient information segregation and integration (Rubinov and Sporns 2010). The presence of small-world reorganization provides a structural foundation for both local and global interactions (Bullmore and Sporns 2009). In the current study, the small-world organizational characteristics were observed in the structural networks and functional networks of both CB and NS group (Watts and Strogatz 1998; Humphries et al. 2006) ($\gamma>1, \lambda\approx1, \sigma>1$). That is to say, with an extended period of network reorganization and cognitive skill acquisition after congenitally visual loss, the structural and functional brain networks of CB group still showed small-world organization, maintaining a balance between integration and segregation overall the whole brain.

Although both groups exhibited small-world organizational characteristics, significant group differences were observed in several topological properties of the structural networks. Specifically, compared to the NS group, the structural network of the CB group showed higher σ and γ values, longer L_p, and lower E_g. These findings are consistent with prior research on the topological properties of structural networks in blind populations (Li et al. 2013; Shu et al. 2009a, b; Zhou et al. 2022) and preterm infants with

early developmental disruption (Zheng et al. 2023; Mousley et al. 2025). And this consistency in the results indicates the reliability of our findings. Specifically, increased L_p and decreased E_g were observed in the structural networks congenital blind individuals (Li et al. 2013). Additionally, increased L_p, decreased E_g (Li et al. 2013; Shu et al. 2009a, b; Zhou et al. 2022), increased σ and γ (Zhou et al. 2022) were observed in the structural networks congenital blind individuals.

The increased γ value, which is the normalized measure of the clustering coefficient (C_p), also indicated enhanced local connectivity. An increase in γ suggests tighter local connections within the structural networks of the CB group, compared with the NS group. Moreover, The observed increased σ value is related with increased γ value while there is no significant alterations in λ value, which is determined by the definition of σ (σ=γ/λ), reflecting similar neural mechanisms of enhanced local connectivity. Together, the higher γ and σ values suggested that congenital visual loss led to tighter local connectivity and improved information synchronization within structural networks, adapting to the lack of visual information, which was the compensatory mechanisms of brain plasticity.

L_p reflects the capacity for efficient information transmission across the brain (Watts and Strogatz 1998). A shorter path length between distant brain regions ensures effective integration and rapid information transmission (Bullmore and Sporns 2009). In this study, a significant increase in L_p was observed in the structural networks of the CB group. This indicated that the average shortest path between any two nodes in the network has lengthened, which implied a decrease in the information propagation efficiency within the structural network. In other words, the congenitally visual loss caused a decrease in the information integration and the ability of neurons to transmit information over long distances. Noting, the apparent discrepancy between the increased L_p and the preserved normalized L_p (λ) in CB group indeed reflects fundamental differences in how real-world brain networks and normalized networks reorganize under sensory deprivation. E_g, which measures the global information transmission efficiency across the entire network, was also reduced in the CB group. The decreased E_g of structural networks in CB group indicated a reduction in the global information transmission and integration (Zhang et al. 2019a, b; Sporns 2011). In summary, the increased L_p and decreased E_g consistently indicated that congenitally visual experience loss led to disruption to the overall properties of the structural networks, affecting through the reduction of global information integration and long-distance information transmission.

These topological reorganizations in structural networks indicated that in order to adapting to visual loss, the brain networks of blind individuals have enhanced local neural connections (i.e., the increase in σ and γ), while there has been a significant decrease in global information transmission efficiency of long-distance connections (i.e., the increase in L_p and the decrease in E_g). To deepen our understanding of the neural mechanisms underlying the network-level topological reorganizations of structural networks, we conducted a more detailed nodal-level topological analysis, in order to reveal the key brain regions responsible for network-level topological alterations of structural network (Supplementary Analysis 1). The findings provided important insights into our understanding of brain plasticity and functional compensation. Firstly, the enhanced local connections induced by the congenitally visual deprivation subserved the information processing of other non-visual sensory modalities, such as the auditory and tactile information (Supplementary Table 3). The enhanced local connections might contributes to improving information processing capacity for the current non-visual modality. Previous study on the string players showed increased local connectivity in the auditory cortex can significantly enhance pitch discrimination abilities (Elbert et al. 1995). Additionally, the reduction of global information transmission efficiency in CB group was related with the disruption of long-distance connections for "visual" regions (Supplementary Table 4), reflecting the selective abandonment of visual pathways. Significant degeneration occurs in vision-related white matter tracts in blind individuals, such as the optic radiation, inferior longitudinal fasciculus, inferior fronto-occipital fasciculus, and splenium of corpus callosum (Jiao et al. 2024; Shu et al. 2009a, b; Reislev et al. 2016; Levin et al. 2010; Bridge et al. 2009).

Additionally, we observed that the topological reorganization patterns of functional and structural network were not identical. Specifically, we did not find any significant group differences in the topological properties of the functional network, which was consisitent with previous on diseases populations (Chen et al. 2021a, c; Latora and Marchiori 2001; Lin et al. 2020). This suggested that changes in the topological properties induced by congenital blindness were more pronounced in the structural networks than in the functional networks. Our findings showed that the topological properties of structural connectivity were more pronounced to congenitally visual deprivation compared to functional connectivity. The observed differences between two networks may reflect fundamentally technical constraints. FC reflects poly-synaptic connections, while SC reflects large bundles of axon fibers, which was due to its limited sensitivity to proximal connections and crossing fibers (Wedeen et al. 2008). Future investigations should focus on elucidating the neurobiological mechanisms underlying this differential sensitivity.

Disruption of SC–FC coupling related with congenital blindness

The structure and function of brain are spatially highly correlated (Mišić et al. 2016). The brain establishes white matter SC through the anatomical connections of neurons (Hagmann et al. 2008; Sarwar et al. 2021), which support and constrain FC between brain regions (Palop and Mucke 2016; Park and Friston 2013; Suárez et al. 2020). And FC, in turn, influences SC through brain plasticity (Honey et al. 2009, 2010). Extensive evidence have indicated the strong correlation between FC and SC in healthy populations, exhibiting robust SC–FC coupling (Vázquez-Rodríguez et al. 2019; Gu et al. 2021). The SC–FC coupling showed plasticity throughout brain development (Grayson et al. 2014; Supekar et al. 2010).

Most previous studies on blindness have relied on single-modal MRI techniques, revealing plastic reorganization in either the brain structure or function. In contrast, our study utilized multi-modal MRI analysis to investigate the plastic reorganization of SC–FC coupling after congenitally visual experience deprivation. Compared to the tight coupling in the NS group, we observed the disruption of SC–FC coupling within the intra-hemispheric brain networks (i.e., LH network and RH network) in the CB group, which was consistent with previous studies on reorganizations in disease populations (Wu et al. 2023; Pan et al. 2023; Chen et al. 2021a, c; Zhang et al. 2019a, b). The reduction in SC–FC coupling might be related with the cognitive functional reorganizations after visual loss. Previous studies have demonstrated that the "visual" cortex was recruited by other cognitive functions (Bedny et al. 2011, 2015; Striem-Amit et al. 2012; Kanjlia et al. 2016, 2021; Raz et al. 2007), and particularly the newly acquired abilities, such as braille reading (Sadato et al. 1996; Hamilton et al. 2000; Burton et al. 2002, 2012). No significant alterations was observed in the SC–FC coupling of inter-hemispheric network, which might reflect the same technical constrains for the lacking of topological reorganizations in functional networks. While no prior studies have examined the SC–FC coupling of sensory deprivation populations, substantial evidence from neurological and psychiatric disorders demonstrates similar disease-induced network decoupling (Wu et al. 2023; Pan et al. 2023; Zhang et al. 2019a, b; Chen et al. 2021a, c), indirectly supporting our conclusion regarding SC–FC decoupling in congenital blindness.

Compared to single-modal MRI analyses, our multi-modal approach, which integrated structural and functional connectivity, provided a more comprehensive picture of dynamic brain changes (Avena-Koenigsberger et al. 2017). The unique insights provided by this study contribute to our understanding of brain plasticity and functional adaptation, shedding light on the complex interplay between structure and function in the context of congenital blindness.

Acquisition of braille cognitive ability mitigates SC–FC decoupling disruption and maintains brain network stability

The SC–FC coupling in brain networks is associated with the acquisition of cognitive abilities (Suárez et al. 2020; Vázquez-Rodríguez et al. 2019; Medaglia et al. 2018; Grayson et al. 2014; Supekar et al. 2010), which is also influenced by diseases (Wu et al. 2023; Pan et al. 2023; Chen et al. 2021a, c; Hagmann et al. 2010; Zhang et al. 2019a, b) and related to clinical indicators (Cao et al. 2020; Cui et al. 2019). Through utilizing correlation analysis between SC–FC CI values and blindness-related measures, we observed that a longer blindness duration corresponded a larger decoupling between SC and FC. For congenital blindness, years of blindness duration and age are necessarily identical. While developmental studies of normal sighted individuals reveal progressive strengthening of SC–FC coupling (Feng et al. 2024; Zimmermann et al. 2016) throughout the same age bracket. This marked difference strongly implicated the influence of blindness duration on the SC–FC coupling in congenitally blindness. Moreover, we also found that the SC–FC coupling was negatively correlated with the age of braille onset and positively correlated with braille reading performance. The SC–FC coupling was increased with the growth of age in normal sighted populations (Feng et al. 2024; Zimmermann et al. 2016), suggesting a higher FC-SC coupling is a normal state for human. Additionally, previous studies in typical populations have established that stronger SC–FC coupling typically accompany enhanced cognitive processing (Suárez et al. 2020; Vázquez-Rodríguez et al. 2019; Popp et al. 2024; Wang et al. 2015a, b). This suggests that braille reading mitigate network decoupling and the brain network of congenitally blind individuals recovery to approaching normal state. These findings in current study indicates while congenitally visual loss disrupted brain networks, the acquisition of braille reading ability mitigated the disruption and maintained the stability brain networks.

In other words, our findings indicated that the CB individuals experienced a large-scale disruption in the structure and function of brain networks, resulting in a decoupling of SC and FC. The longer duration of visual experience deprivation induced more severe network disruption. However, the acquisition of cognitive abilities associated with braille reading allowed CB individuals to develop alternative perceptual and cognitive strategies to compensate for vision loss. As a result, the brain networks remained stable to some extent, particularly by enhancing the information processing of other sensory pathways.

The current study provides valuable insights for rehabilitation interventions for the blind population. It underscores the importance of learning braille at an early age and achieving proficiency in braille reading. Such efforts can help minimize the impact of blindness on brain network organization, facilitating functional compensation and enhancing overall cognitive adaptation.

Limitations

This study has several limitations that should be addressed in future research. The sample size in this study was relatively small, primarily due to the limited availability of congenitally blind participants. Future studies should consider expanding recruitment efforts and including a larger sample size. Additionally, the current study examined the SC–FC coupling reorganization at both the whole-brain and hemispheric levels, and we did not investigate plastic reorganization of SC–FC coupling at a more granular level, such as the modular or regional level. Future research could reveal the plastic reorganization of SC–FC coupling at these granular level, in order to deeply understand the plastic neural mechanisms in congenital blindness.

Conclusion

Congenital visual experience deprivation induces significant topological changes in structural networks, accompanied by disrupted SC–FC coupling within hemispheric networks. The degree of disruption in SC–FC coupling is influenced by the duration of blindness, with longer deprivation leading to more severe decoupling. However, the acquisition of braille reading ability partially mitigates this disruption. These findings offer a deeper understanding of dynamic changes in brain network structure and information integration.

Supplementary Information The online version contains supplementary material available at https://doi.org/10.1007/s00429-025-02975-9.

Acknowledgements This work was supported by the Major Project of National Social Science Foundation (24&ZD252) and National Natural Science Foundation of China (32271091 and 82372555). We would like to thank the members of the BNU-Han Lab for their supports and all participants for their cooperation.

Author contributions Saiyi Jiao: Conceptualization, Methodology, Formal analysis, Investigation, Data curation, Writing– original draft, Writing– review & editing, Visualization. Ke Wang: Investigation. Jiahong Zeng: Data curation. Zhenjiang Cui: Data curation. Yudan Luo: Visualization. Zaizhu Han: Conceptualization, Investigation, Writing–review & editing, Supervision, Funding acquisition.

Data availability Data will be made available from the corresponding author on reasonable request.

Declarations

Competing interests The authors declare no competing interests.

References

Ashburner J (2007) A fast diffeomorphic image registration algorithm. NeuroImage 38:95–113

Avena-Koenigsberger A, Misic B, Sporns O (2017) Communication dynamics in complex brain networks. Nat Rev Neurosci 19:17–33

Bedny M, Pascual-Leone A, Dodell-Feder D, Fedorenko E, Saxe R (2011) Language processing in the occipital cortex of congenitally blind adults. Proc Natl Acad Sci U S A 108:4429–4434

Bedny M, Richardson H, Saxe R (2015) Visual cortex responds to spoken Language in blind children. J Neurosci 35:11674–11681.

Bridge H, Cowey A, Ragge N, Watkins K (2009) Imaging studies in congenital anophthalmia reveal preservation of brain architecture in 'visual' cortex. Brain 132:3467–3480

Bullmore E, Sporns O (2009) Complex brain networks: graph theoretical analysis of structural and functional systems. Nat Rev Neurosci 10:186–198

Burton H, Snyder AZ, Conturo TE, Akbudak E, Ollinger JM, Raichle ME (2002) Adaptive changes in early and late blind: a fMRI study of braille reading. J Neurophysiol 87:589–607

Burton H, Sinclair RJ, Agato A (2012) Recognition memory for braille or spoken words: an fMRI study in early blind. Brain Res 1438:22–34

Cao R, Wang X, Gao Y, Li T, Zhang H, Hussain W, Xie Y, Wang J, Wang B, Xiang J (2020) Abnormal anatomical Rich-Club organization and structural-functional coupling in mild cognitive impairment and Alzheimer's disease. Front Neurol 11:53

Chen H, Geng W, Shang S, Shi M, Zhou L, Jiang L, Wang P, Yin X, Chen Y (2021a) Alterations of brain network topology and structural connectivity-functional connectivity coupling in capsular versus Pontine stroke. Euro J Neurol 28:1967–1976

Chen Q, Lv H, Wang Z, Wei X, Zhao P, Yang Z, Gong S, Wang Z (2021b) Outcomes at 6 months are related to brain structural and white matter microstructural reorganization in idiopathic tinnitus patients treated with sound therapy. Hum Brain Mapp 42:753–765

Chen Q, Lv H, Wang Z, Wei X, Liu J, Liu F, Zhao P, Yang Z, Gong S, Wang Z (2022) Distinct brain structural-functional network topological coupling explains different outcomes in tinnitus patients treated with sound therapy. Hum Brain Mapp 43:3245–3256

Chiang S, Stern JM, Engel J, Haneef Z (2015) Structural-functional coupling changes in Temporal lobe epilepsy. Brain Res 1616:45–57

Cui Z, Zhong S, Xu P, He Y, Gong G (2013) PANDA: a pipeline toolbox for analyzing brain diffusion images. Front Hum Neurosci 7

Cui L-B, Wei Y, Xi Y-B, Griffa A, De Lange SC, Kahn RS, Yin H, Van den Heuvel MP (2019) Connectome-Based patterns of First-Episode Medication-Naïve patients with schizophrenia. Schizophr Bull 45:1291–1299

Damoiseaux JS, Greicius MD (2009) Greater than the sum of its parts: a review of studies combining structural connectivity and resting-state functional connectivity. Brain Struct Funct 213:525–533

Damoiseaux JS, Rombouts S a. RB, Barkhof F, Scheltens P, Stam CJ, Smith SM, Beckmann CF (2006) Consistent resting-state networks across healthy subjects. Proc Natl Acad Sci U S A 103:13848–13853

Elbert T, Pantev C, Wienbruch C, Rockstroh B, Taub E (1995) Increased cortical representation of the fingers of the left hand in string players. Science 270:305–307

Fan L, Li H, Zhuo J, Zhang Y, Wang J, Chen L, Yang Z, Chu C, Xie S, Laird AR, Fox PT, Eickhoff SB, Yu C, Jiang TFan L et al (2016) The human brainnetome atlas: A new brain atlas based on connectional architecture. Cereb Cortex 26(8):3508–3526

Feng G, Wang Y, Huang W, Chen H, Cheng J, Shu N (2024) Spatial and temporal pattern of structure–function coupling of human brain connectome with development. eLife 13:RP93325

Grayson DS, Ray S, Carpenter S, Iyer S, Dias TGC, Stevens C, Nigg JT, Fair DA (2014) Structural and functional rich club organization of the brain in children and adults. PLoS ONE 9:e88297

Greenough WT, Black JE, Wallace CS (1987) Experience and brain development. Child Dev 58:539

Gu Z, Jamison KW, Sabuncu MR, Kuceyeski A (2021) Heritability and interindividual variability of regional structure-function coupling. Nat Commun 12:4894

Hagmann P, Cammoun L, Gigandet X, Meuli R, Honey CJ, Wedeen VJ, Sporns O (2008) Mapping the structural core of human cerebral cortex. PLoS Biol 6:e159

Hagmann P, Sporns O, Madan N, Cammoun L, Pienaar R, Wedeen VJ, Meuli R, Thiran J-P, Grant PE (2010) White matter maturation reshapes structural connectivity in the late developing human brain. Proc Natl Acad Sci U S A 107:19067–19072

Hamilton R, Keenan JP, Catala M, Pascual-Leone A (2000) Alexia for braille following bilateral occipital stroke in an early blind woman. NeuroReport 11:237–240

Honey CJ, Sporns O, Cammoun L, Gigandet X, Thiran JP, Meuli R, Hagmann P (2009) Predicting human resting-state functional connectivity from structural connectivity. Proc Natl Acad Sci U S A 106:2035–2040

Honey CJ, Thivierge J-P, Sporns O (2010) Can structure predict function in the human brain? Neuroimage 52:766–776

Hou F, Liu X, Zhou Z, Zhou J, Li H (2017) Reduction of interhemispheric functional brain connectivity in early blindness: a resting-state fMRI study. BioMed Res Int 2017:6756927

Huang H, Ding M (2016) Linking functional connectivity and structural connectivity quantitatively: a comparison of methods. Brain Connect 6:99–108

Humphries MD, Gurney K, Prescott TJ (2006) The brainstem reticular formation is a small-world, not scale-free, network. Proc Biol Sci 273:503–511

Jenkinson M, Bannister P, Brady M, Smith S (2002) Improved optimization for the robust and accurate linear registration and motion correction of brain images. NeuroImage 17:825–841

Jiao S, Wang K, Zhang L, Luo Y, Lin J, Han Z (2023) Developmental plasticity of the structural network of the occipital cortex in congenital blindness. Cereb Cortex 33:11526–11540

Jiao S, Wang K, Luo Y, Zeng J, Han Z (2024) Plastic reorganization of the topological asymmetry of hemispheric white matter networks induced by congenital visual experience deprivation. NeuroImage 299:120844

Joukal M (2017) Anatomy of the human visual pathway. In: Skorkovská K (ed) Homonymous visual field defects. Springer International Publishing, Cham, pp 1–16.

Kanjlia S, Lane C, Feigenson L, Bedny M (2016) Absence of visual experience modifies the neural basis of numerical thinking. Proc Natl Acad Sci U S A 113:11172–11177

Kanjlia S, Loiotile RE, Harhen N, Bedny M (2021) 'Visual' cortices of congenitally blind adults are sensitive to response selection demands in a go/no-go task. NeuroImage 236:118023

Knijnenburg TA, Wessels LFA, Reinders MJT, Shmulevich I (2009) Fewer permutations, more accurate *P* -values. Bioinformatics 25:i161–i168

Kolb B (1998) Age, Experience and the changing brain. Neurosci Biobehavioral Reviews 22:143–159

Kuceyeski A, Shah S, Dyke JP, Bickel S, Abdelnour F, Schiff ND, Voss HU, Raj A (2016) The application of a mathematical model linking structural and functional connectomes in severe brain injury. Neuroimage Clin 11:635–647

Latora V, Marchiori M (2001) Efficient behavior of Small-World networks. Phys Rev Lett 87:198701

Leemans A, Jones DK (2009) The *B* -matrix must be rotated when correcting for subject motion in DTI data. Magn Reson Med 61:1336–1349

Levin N, Dumoulin SO, Winawer J, Dougherty RF, Wandell BA (2010) Cortical maps and white matter tracts following long period of visual deprivation and retinal image restoration. Neuron 65:21–31

Li J, Liu Y, Qin W, Jiang J, Qiu Z, Xu J, Yu C, Jiang T (2013) Age of onset of blindness affects brain anatomical networks constructed using diffusion tensor tractography. Cereb Cortex 23:542–551

Li M, Liu T, Xu X, Wen Q, Zhao Z, Dang X, Zhang Y, Wu D (2022) Development of visual cortex in human neonates is selectively modified by postnatal experience. eLife 11:e78733

Lin S-Y, Eaton NR, Schleider JL (2020) Unpacking associations between mood symptoms and screen time in preadolescents: a network analysis. J Abnorm Child Psychol 48:1635–1647

Lin J, Zhang L, Guo R, Jiao S, Song X, Feng S, Wang K, Li M, Luo Y, Han Z (2022) The influence of visual deprivation on the development of the thalamocortical network: evidence from congenitally blind children and adults. NeuroImage 264:119722

Maslov S, Sneppen K (2002) Specificity and stability in topology of protein networks. Science 296:910–913

McKenzie IA, Ohayon D, Li H, Paes de Faria J, Emery B, Tohyama K, Richardson WD (2014) Motor skill learning requires active central myelination. Science 346:318–322

Medaglia JD, Huang W, Karuza EA, Kelkar A, Thompson-Schill SL, Ribeiro A, Bassett DS (2018) Functional alignment with anatomical networks is associated with cognitive flexibility. Nat Hum Behav 2:156–164

Milo R, Shen-Orr S, Itzkovitz S, Kashtan N, Chklovskii D, Alon U (2002) Network motifs: simple Building blocks of complex networks. Science 298:824–827

Mišić B, Betzel RF, de Reus MA, van den Heuvel MP, Berman MG, McIntosh AR, Sporns O (2016) Network-Level Structure-Function relationships in human neocortex. Cereb Cortex 26:3285–3296

Mori S, van Zijl PCM (2002) Fiber tracking: principles and strategies - a technical review. NMR Biomed 15:468–480

Mori S, Crain BJ, Chacko VP, van Zijl PCM (1999) Three-dimensional tracking of axonal projections in the brain by magnetic resonance imaging. Ann Neurol 45:265–269

Mousley A, Akarca D, Astle DE (2025) Premature birth changes wiring constraints in neonatal structural brain networks. Nat Commun 16:490

Oldfield RC (1971) The assessment and analysis of handedness: the Edinburgh inventory. Neuropsychologia 9:97–113

Palop JJ, Mucke L (2016) Network abnormalities and interneuron dysfunction in alzheimer disease. Nat Rev Neurosci 17:777–792

Pan Y, Li X, Liu Y, Jia X, Wang S, Ji Q, Zhao W, Yin B, Bai G, Zhang J, Bai L (2023) Hierarchical brain structural–functional coupling associated with cognitive impairments in mild traumatic brain injury. Cereb Cortex 33:7477–7488

Park H-J, Friston K (2013) Structural and functional brain networks: from connections to cognition. Science 342:1238411

Pelland M, Orban P, Dansereau C, Lepore F, Bellec P, Collignon O (2017) State-dependent modulation of functional connectivity in early blind individuals. NeuroImage 147:532–541

Pinotsis DA, Hansen E, Friston KJ, Jirsa VK (2013) Anatomical connectivity and the resting state activity of large cortical networks. NeuroImage 65:127–138

Popp JL, Thiele JA, Faskowitz J, Seguin C, Sporns O, Hilger K (2024) Structural-functional brain network coupling predicts human cognitive ability. NeuroImage 290:120563

Raz N, Striem E, Pundak G, Orlov T, Zohary E (2007) Superior serial memory in the blind: A case of cognitive compensatory adjustment. Curr Biol 17:1129–1133

Reislev NL, Kupers R, Siebner HR, Ptito M, Dyrby TB (2016) Blindness alters the microstructure of the ventral but not the dorsal visual stream. Brain Struct Funct 221:2891–2903

Romero-Garcia R, Atienza M, Cantero JL (2014) Predictors of coupling between structural and functional cortical networks in normal aging. Hum Brain Mapp 35:2724–2740

Rubinov M, Sporns O (2010) Complex network measures of brain connectivity: uses and interpretations. NeuroImage 52:1059–1069

Sadato N, Pascual-Leone A, Grafman J, Ibañez V, Deiber M-P, Dold G, Hallett M (1996) Activation of the primary visual cortex by braille reading in blind subjects. Nature 380:526–528

Sampaio-Baptista C, Johansen-Berg H (2017) White matter plasticity in the adult brain. Neuron 96:1239–1251

Sarwar T, Tian Y, Yeo BTT, Ramamohanarao K, Zalesky A (2021) Structure-function coupling in the human connectome: A machine learning approach. NeuroImage 226:117609

Shu N, Liu Y, Li J, Li Y, Yu C, Jiang T (2009a) Altered anatomical network in early blindness revealed by diffusion tensor tractography. PLoS ONE 4:e7228

Shu N, Li J, Li K, Yu C, Jiang T (2009b) Abnormal diffusion of cerebral white matter in early blindness. Hum Brain Mapp 30:220–227

Sporns O (2011) The human connectome: a complex network. Ann N Y Acad Sci 1224:109–125

Striem-Amit E, Cohen L, Dehaene S, Amedi A (2012) Reading with sounds: sensory substitution selectively activates the visual word form area in the blind. Neuron 76:640–652

Suárez LE, Markello RD, Betzel RF, Misic B (2020) Linking structure and function in macroscale brain networks. Trends Cogn Sci 24:302–315

Supekar K, Uddin LQ, Prater K, Amin H, Greicius MD, Menon V (2010) Development of functional and structural connectivity within the default mode network in young children. NeuroImage 52:290–301

Townsend J, Ashby G, Ashby G, Ashby G (1983) Stochastic modeling of elementary psychological processes. CUP Archive

Ungewiss J, Breuninger T, Milenkovic I, Ebenhoch R, Schiefer U (2020) Aufbau und funktion der Sehbahn. Ophthalmologe 117:1062–1067

van den Heuvel MP, Sporns O (2011) Rich-Club organization of the human connectome. J Neurosci 31:15775–15786

van den Heuvel MP, Sporns O, Collin G, Scheewe T, Mandl RCW, Cahn W, Goñi J, Hulshoff Pol HE, Kahn RS (2013) Abnormal rich club organization and functional brain dynamics in schizophrenia. JAMA Psychiatry 70:783–792

Vázquez-Rodríguez B, Suárez LE, Markello RD, Shafiei G, Paquola C, Hagmann P, van den Heuvel MP, Bernhardt BC, Spreng RN, Misic B (2019) Gradients of structure-function tethering across neocortex. Proc Natl Acad Sci U S A 116:21219–21227

Wang Z, Dai Z, Gong G, Zhou C, He Y (2015a) Understanding structural-functional relationships in the human brain: a large-scale network perspective. Neuroscientist 21:290–305

Wang J, Wang X, Xia M, Liao X, Evans A, He Y (2015b) GRETNA: a graph theoretical network analysis toolbox for imaging connectomics. Front Hum Neurosci 9.

Wang X, Lin Q, Xia M, He Y (2018) Differentially categorized structural brain hubs are involved in different microstructural, functional, and cognitive characteristics and contribute to individual identification. Hum Brain Mapp 39:1647–1663

Wang S, Gan S, Yang X, Li T, Xiong F, Jia X, Sun Y, Liu J, Zhang M, Bai L (2021) Decoupling of structural and functional connectivity in hubs and cognitive impairment after mild traumatic brain injury. Brain Connect 11:745–758

Watts DJ, Strogatz SH (1998) Collective dynamics of 'small-world' networks. Nature 393:440–442

Wedeen VJ, Wang RP, Schmahmann JD, Benner T, Tseng WYI, Dai G, Pandya DN, Hagmann P, D'Arceuil H, de Crespigny AJ (2008) Diffusion spectrum magnetic resonance imaging (DSI) tractography of crossing fibers. NeuroImage 41:1267–1277

Wu J, He Y, Liang S, Liu Z, Huang J, Liu W, Tao J, Chen L, Chan CCH, Lee TMC (2023) Effects of computerized cognitive training on structure–function coupling and topology of multiple brain networks in people with mild cognitive impairment: a randomized controlled trial. Alzheimers Res Ther 15:158

Zhang R, Shao R, Xu G, Lu W, Zheng W, Miao Q, Chen K, Gao Y, Bi Y, Guan L, McIntyre RS, Deng Y, Huang X, So K-F, Lin K (2019a) Aberrant brain structural-functional connectivity coupling in euthymic bipolar disorder. Hum Brain Mapp 40:3452–3463

Zhang X, Yu X, Bao Q, Yang L, Sun Y, Qi P (2019b) Multimodal neuroimaging study reveals dissociable processes between structural and functional networks in patients with subacute intracerebral hemorrhage. Med Biol Eng Comput 57:1285–1295

Zhao C, Yang L, Xie S, Zhang Z, Pan H, Gong G (2019) Hemispheric module-specific influence of the X chromosome on white matter connectivity: evidence from girls with Turner syndrome. Cereb Cortex 29:4580–4594

Zheng W, Wang X, Liu T, Hu B, Wu D (2023) Preterm-birth alters the development of nodal clustering and neural connection pattern in brain structural network at term-equivalent age. Hum Brain Mapp 44:5372–5386

Zhong S, He Y, Gong G (2015) Convergence and divergence across construction methods for human brain white matter networks: an assessment based on individual differences. Hum Brain Mapp 36:1995–2013

Zhou Z, Qian L, Xu J, Lu Y, Hou F, Zhou J, Luo J, Hou G, Jiang W, Li H, Liu X (2022) Topologic reorganization of white matter connectivity networks in early-blind adolescents. Neural Plasticity 2022:1–11

Zimmermann J, Ritter P, Shen K, Rothmeier S, Schirner M, McIntosh AR (2016) Structural architecture supports functional organization in the human aging brain at a regionwise and network level. Hum Brain Mapp 37:2645–2661